Jurnal Teknologi

Design and Analysis of Rigid-Body Shape-Change Mechanism for Aircraft Wings

Mohammad Hazrin Ismail[a*], Shamsul Anuar Shamsudin[a,b], Mohd Nizam Sudin[a,b]

[a]Centre for Advanced Research on Energy, Universiti Teknikal Malaysia Melaka
[b]Faculty of Mechanical Engineering, Unversiti Teknikal Malaysia Melaka

*Corresponding author
mohammadhazrin858@gmail.com

Graphical abstract
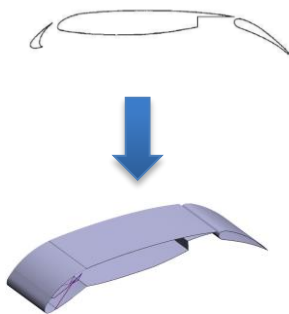
Abstract

Airframe noise reduction becomes a main interest among researchers who study the performance of aircrafts. The airframe noise can occur between the high-lift systems and main body of the airfoil. The proposed shape-changing airfoil is one of many ideas to reduce airframe noise by eliminating the gap between the main body and high-lift systems. This paper presents a new design of 30P30N airfoil, which converts the three-element airfoil (slat, main body and flap) into two-element airfoil (combination of slat and main body as an element and flap) by installing a shape-changing slat into the systems. This work applies a chain of rigid bodies connected by revolute and prismatic joints that are capable of approximating a shape change defined by a set of morphed slat design profiles. To achieve a single degree of freedom (DOF), a building-block approach is employed to mechanize the fixed-end shape-changing chain with the helped of Geometric Constraint Programming technique as an effective method to develop the mechanism. The conventional and shape-change 30P30N airfoils are compared to study the performances of airfoils with the velocity and angle of attack are constant.

Keywords: Kinematic Synthesis; shape-changing mechanism; geometric constraint programming; aerodynamic performance; coefficient of pressure

Abstrak

Pengurangan bunyi kerangka pesawat udara menjadi fokus utama di kalangan penyelidik yang mengkaji prestasi pesawat. Aerofoil ubah-bentuk telah dicadangkan untuk mengurangkan bunyi kerangka pesawat udara dengan menghapuskan jurang antara sistem daya angkat tinggi dan badan utama aerofoil. Kertas kerja ini membentangkan reka bentuk baru aerofoil 30P30N, yang menukarkan aerofoil dari tiga elemen (slat, badan utama dan flap) kepada dua elemen (gabungan slat dan bdan utama sebagai satu elemen dan flap) dengan memasang slat ubah-bentuk ke dalam sistem. Ia mengaplikasikan rantaian jasad tegar yang dihubungkan dengan sendi revolute dan prismatik yang mampu memghampiri ubah bentuk yang didefinisikan dari satu set profil reka bentuk slat berubah. Untuk mencapai satu darjah kebebasan (DOF), pendekatan blok-bangunan digunakan untuk menggerakkan rantaian ubah-bentuk hujung kekal dengan bantuan pengaturcara kekangan geometri untuk membangunkan mekanisma. Aerofoil 30P30N konvensional dan ubah-bentuk dibandingkan untuk mengkaji prestasi aerofoil dimana halaju dan sudut serangan adalah malar.

Kata kunci: Sintesis kinematik; mekanisma ubah-bentuk; pengaturcara kekangan geometri; prestasi aerodinamik; pekali tekanan

1.0 INTRODUCTION

High-lift systems (slats and flaps) play an important role in aircraft performance and they are widely used during takeoff and landing. Despite its important roles, conventional high-lift systems have some issues that affect the aircraft performance. Firstly, a high-lift system is a part of multi-element airfoil where it has three elements; one element is the main body and two elements are the high-lift systems.

Past studies have suggested that the high-lift systems and landing gears are the main noise producing components of airframe noise [1-2]. Khorrami [3] studied on the major noise generation mechanisms that are related to the slat. In the study, the focus was on the important of role of computational simulations in identification and understanding of noise sources. Previous studies stated that the gap between the high-lift systems (slat and flap) and solid walls (main body) contributes the airframe noise generation [4-5]. Morrison [6] reported on a numerical study done by NASA on the 30P30N airfoil with three-element high-lift configurations. The report showed an increase in pressure near the gap between the slat and the main wing body.

Some actions can be taken to solve the issues on the high-lift systems. Hence, having a novel slat that extends out as usual but covers the gap can be achieved with the chain of shape-changing rigid-bodies. The use of shape-changing mechanism on aircraft wing [7-8] that utilizes rigid-body segments that form a closed-chain connected by revolute joints eliminating the gap between the main components. Shamsudin [9] proposed and developed a shape-changing mechanisms focused on the slat of 30P30N airfoil.

In this paper, a three-element airfoil is redesigned into a two-element airfoil by introducing shape-change mechanism. The slat and main body are combined as one body where shape-changing slat is applied to the main body. The synthesis process is started with a segmentation phase that creates segments, which are optimized in shape and length so that they approximate corresponding portions on each desired profile. To complete the synthesis, a mechanization phase applies building-block approach to a selected segment and adds binary or ternary link in order to achieve a lower degree-of-freedom (DOF) linkage. If possible, a 1-DOF system is preferred for simplicity in control. Then, an analysis is performed on the new airfoil with the focus on slat area to compare with the conventional multi-element airfoil based on the static pressure P_∞, velocity v, and coefficient of pressure C_P, along the both airfoils.

The paper is organized as follows: Section 2 presents the overview of the conventional and current shape-changing slat of 30P30N airfoil. Section 3 discusses the numerical simulation and computational setup of slat-airfoil configuration. Section 4 details the results obtained for shape-changing and conventional 30P30N airfoils. Finally, Section 5 proposes concluding remarks.

2.0 OVERVIEW OF RIGID-BODIES SHAPE-CHANGE MECCHANISM

Developed by McDonnell Douglas, the 30P30N airfoil was selected in this study because it is widely documented with both experimental and numerical results. The selected airfoil can be categorized as a multi-element airfoil where it consists of three elements; main body, slat, and flap. Figure 1 shows the 30P30N airfoil profile used in the current study. Ramsey and Ying [10] gave a detailed review on the CFD methods applied to compute the high-lift multi-element airfoil. Meanwhile, Li Fang's comparative study [11] provided in-depth analysis of aerodynamic performance on two-element airfoil when upper-surface blowing is applied on flap configuration.

Figure 1 Wing profile of 30P30N airfoil [10]

2.1 Conventional Slat Mechanism

An example of a conventional slat mechanism is shown in Figure 2. A driver shaft (part 1) can rotates the two pinions (parts 2 and 3) that have different radii. Then the slat is deployed forward by one drive arm attached to a rack and rotated by the push of another faster moving drive arm attached to a different rack.
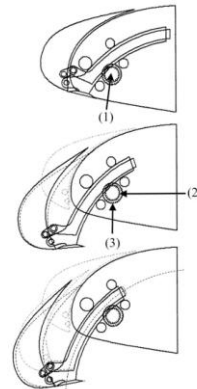
Figure 2 The two rack and pinion systems drive the slat out the wing

2.2 New Slat Mechanism

The new slat mechanism is proposed by converting the type of slat from split type to one that hinged to

the main body of airfoil. The process starts with segmenting the slat profiles using ShapeChanger, a MATLAB-based application to perform all segmentations shown in this work including the process to create a chain of rigid body segments. This work is based on matrix where the design vector dictates the creation of an initial segment matrix and specifies the segment types (M– and C–segments) in the chain. Mean segment (M– segment) is a segment that contains the same number of points in all instances on each target profile while constant curvature segment (C–segment) is a segment that consists of different number of points in all instances on each profile [9]. The segment distance errors are calculated to improve the unconnected segments. The process can be repeated with other design vectors and tried with many starting guesses. The set of segments can be connected and each instance of segment location optimized versus the set of target profiles.

A set of rigid-body segments is generated through the segmentation process using ShapeChanger. These segments are then joined together to form as a linkage, where the prismatic joints are attached in between the prismatic links.   Meanwhile, the remainder links are connected together at the end points with the revolute joints. In order to achieve 1-DOF for mechanism with prismatic joint, the application of building-block approach [12] is needed for mechanization stage as it is widely accepted for analysis [13-14] and synthesis [15,16] of planar mechanism. The rigid segments are constructed in the sketching mode of a parametric design software package, and geometric constraint programming (GCP) [17] techniques are employed.

Figure 3a through 3c show the movement of the mechanisms by a single-DOF system. Figure 3a shows the dyad link as the input, which can also be connected to a shorter crank link (not shown) that is able to complete a full revolution. This input dyad is selected as it is short, moves monotonically, and is nearest to the main actuator that is situated in the main wing element. Figure 4 shows the slat 30P30N is designed from CATIA software.

3.0 SIMULATION SETUP

3.1 Sketching Simulation Setup

The shape-changing slat design first is converted into 3D model using the CATIA V5R20 software. The full-scale model in CAD is developed to see the movement of mechanisms from a cruise state into landing state. The sketching is made using sketching environment in CATIA V5R20. The overall 3D profiles of shape-changing 30P30N are projected to the XY plane as the slat and flap are on the landing state. The sketched profile then converted into surface and saved as IGES file so it can be readable in the ANSYS Fluent CFD package.

(a)

(b)

(c)
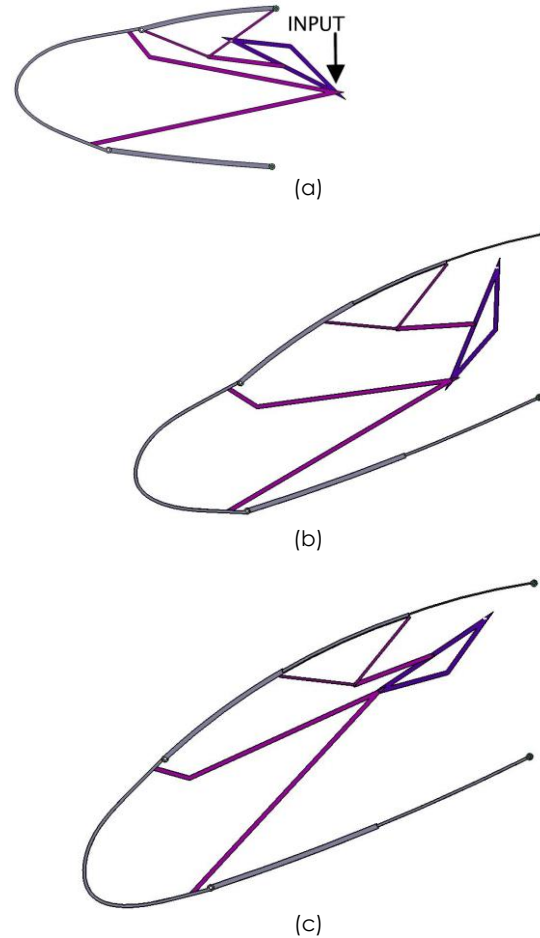
Figure 3 The movement of slat mechanisms for (a) A fully stowed slat at 0º. (b) An interim position as it approaches the deployed position at 15º. (c) The fully deployed (extended) slat at 30º.
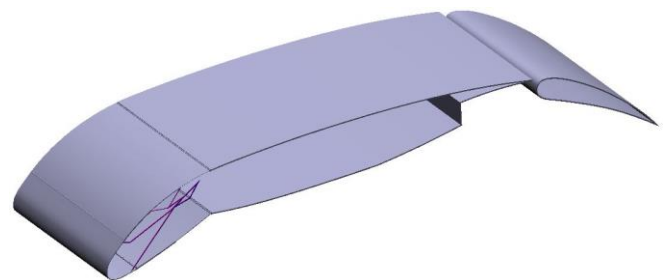
Figure 4 The movement of slat

3.2 Numerical Strategy

The detailed of aerodynamic performance of the airfoil is shown through the coefficient of pressure along the airfoil. In this simulation, the linearized pressure coefficient formula is used for $M_\infty < 0.5$ since the simulation has $M_\infty = 0.2$.

First, let define the pressure coefficient C_P over the wing as follows:

$$C_p = \frac{P - P_\infty}{Q_\infty} = \frac{P - P_\infty}{\frac{1}{2}\rho_\infty V_\infty^2} \tag{1}$$

where P_∞ and P represent the static pressures in the freestream and pressure at any point while Q_∞ represent the dynamic pressure. The dynamic pressure also can be expressed in term of M_∞ as in

$$Q_\infty = \frac{1}{2}\rho_\infty V_\infty^2 = \frac{1}{2}\frac{\gamma P_\infty}{\gamma P_\infty}\rho_\infty V_\infty^2 = \frac{\gamma}{2}P_\infty\left(\frac{\rho_\infty}{\gamma P_\infty}\right)V_\infty^2. \tag{2}$$

Equation (2) can be substituted with $a_\infty^2 = \gamma P_\infty / \rho_\infty$. Thus, becomes

$$Q_\infty = \frac{\gamma}{2}P_\infty\frac{V_\infty^2}{a_\infty^2} = \frac{\gamma}{2}P_\infty M_\infty^2. \tag{3}$$

Substituting (3) into (1), then the coefficient of of pressure at any point on the airfoil's body becomes

$$C_p = \frac{2}{\gamma M_\infty^2}\left(\frac{P}{P_\infty} - 1\right). \tag{4}$$

3.3 Computational Setup

The computational analysis of 2D case was carried out for a landing configuration with slat and flap deflections of 30° and angle of attack (AoA) of 10° at a Mach number of 0.21 for a Reynolds number of 4.5 million based on mean aerodynamic chord. The mean aerodynamic chord is 1.01 m and model semi-span is 2.16 m.

The simulation is conducted using pressure-based solver in the steady state that solves the equation of energy, momentum, and continuity at the initial state. The use of model of realizable k-epsilon with Non-equilibrium wall function in the simulation since the model is simple and stable for the initial simulation strategy.

At the same time, the sketch of conventional 30P30N airfoil was prepared also using CATIA V5R20 software and then simulated on ANSYS Fluent where all the parameters are the same as that of the shape-changing 30P30N airfoil.

4.0 RESULTS AND DISCUSSION

The results of the simulations are reported in this section. First, the contours of static pressure and velocity around the airfoil will be presented. Then, the graphs of coefficient of pressure for both airfoils will be compared. Lastly, the SPL values will be shown and discussed.

Fig. 5a through 5d show the contours of static pressure along the airfoil body for both shape-changing and conventional 30P30N airfoils. Both airfoils have high values of static pressure at leading edge (stagnation point). The lower surface of shape-changing airfoil shows constant high pressure that contributes to better lift coefficient compared to conventional airfoil. Besides, for the conventional airfoil, the gap between the slat and main body affects the static pressure on the upper surface as a very low static pressure is computed there. Although the conventional airfoil has higher pressure value compared to shape-changing airfoil at certain area, but the great difference between the highest and lowest pressure affects the pressure distribution along the main airfoil.

Meanwhile, Fig. 6a through 6d present the contours of velocity along the airfoil body for both types of airfoils. The shape-changing airfoil has high velocity at the upper surface of the slat (including the region where the gap between slat and main body is eliminated), constant velocity along other body surface and low velocity at the trailing edge region. On the other hand, a very low velocity occurs at the gap between slat and main body of conventional airfoil while a high velocity is calculated as the air is passing through the gap to the upper surface of main body. From the results, the shape-changing airfoil has average air velocity in between 3.84 m/s^{-1} to 6.53 m/s^{-1} at the lower surface of airfoil, which is lower than the conventional airfoil at 8.75 m/s^{-1} to 13.29 m/s^{-1}.

From the simulation, the surface pressure data along the airfoil body can be recorded. Fig. 7a and 7b show the graph of coefficient of pressure along the airfoil body against the point coordinates at the airfoil body for shape-changing and conventional 30P30N airfoil. Shape-changing airfoil has the higher suction pressure on the upper surface of leading edge while for the conventional airfoil has the higher suction pressure at the end of the upper surface of main body.

Fig. 8a and 8b present the comparison of Surface Pressure Level SPL between both conventional and shape-changing airfoils. From Fig.8a, the upper surface of shape-changing airfoil has constantly high SPL value but low SPL value at the lower surface of airfoil. Meanwhile, the conventional airfoil has inconsistent SPL value around the airfoil's body with the area within the slat and main body has the higher SPL value. From the both results, the value of SPL at the stagnation point of the shape-changing airfoil is lower compared to the conventional airfoil.

From both results, the shape-changing airfoil gives enormous decrease in term of noise reduction in slat area. Compare to conventional airfoil, this gapless slat airfoil reduces the slat noise up to 40 dB especially on the area around lower slat surface. Consequently, the results also conclude that the performance of the propose system match significantly with previous work done by [18-19].
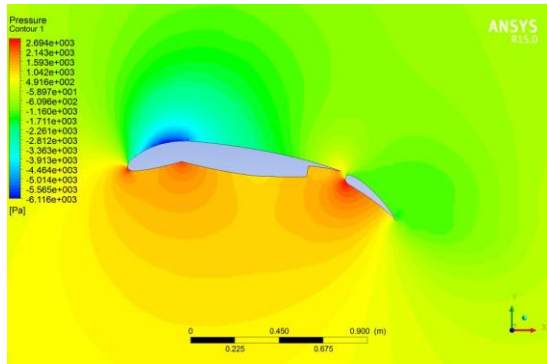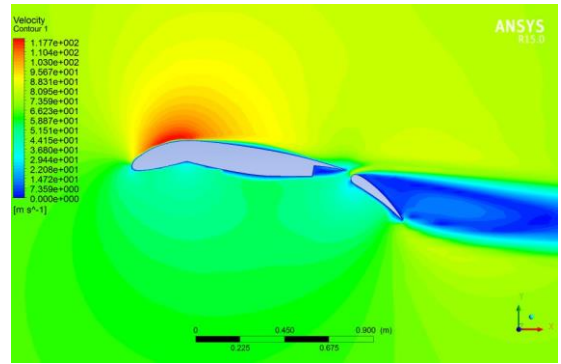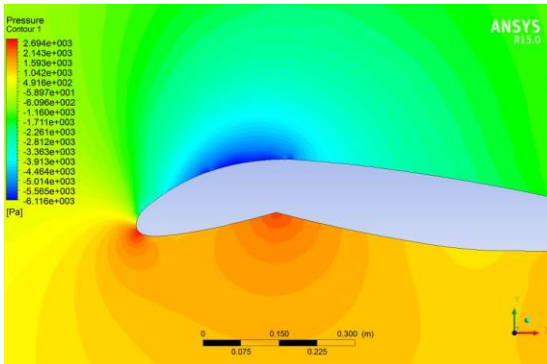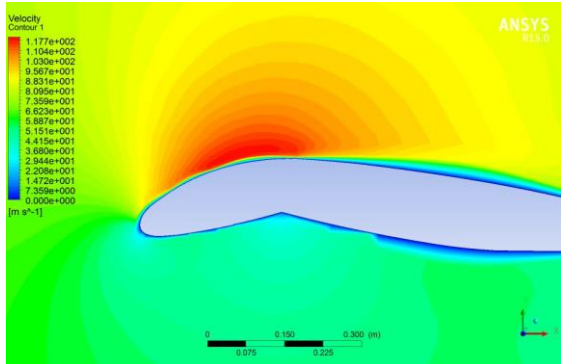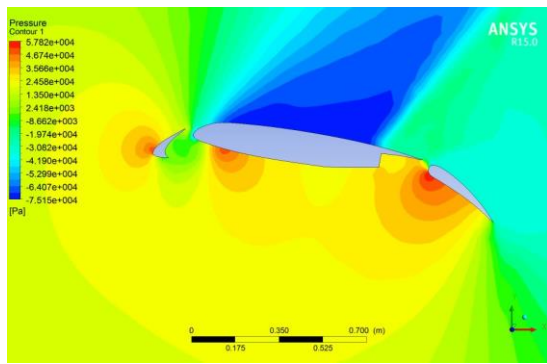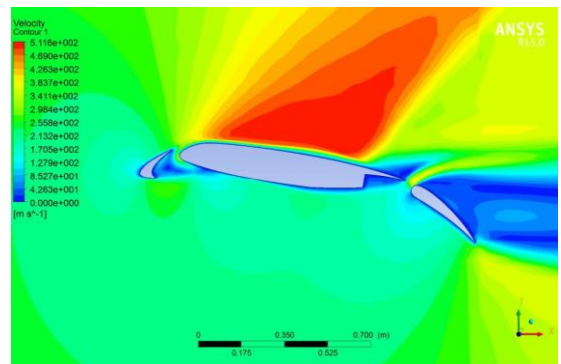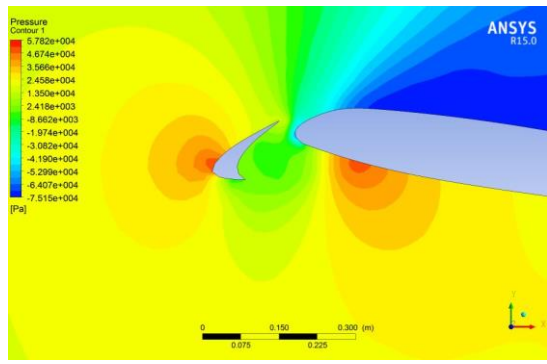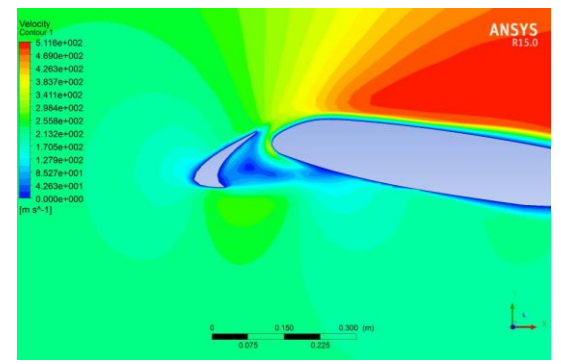
Figure 5 (a) Overall static pressure along shape-changing airfoil (b) Static pressure around slat region of shape-changing airfoil (c) Overall static pressure along conventional airfoil (d) Static pressure around slat region of conventional airfoil

Figure 6 (a) Overall velocity along the shape-changing airfoil (b) Velocity around the slat region of shape-changing airfoil (c) Overall velocity along the conventional airfoil (d) Velocity around the slat region of conventional airfoil

(a)   (b)
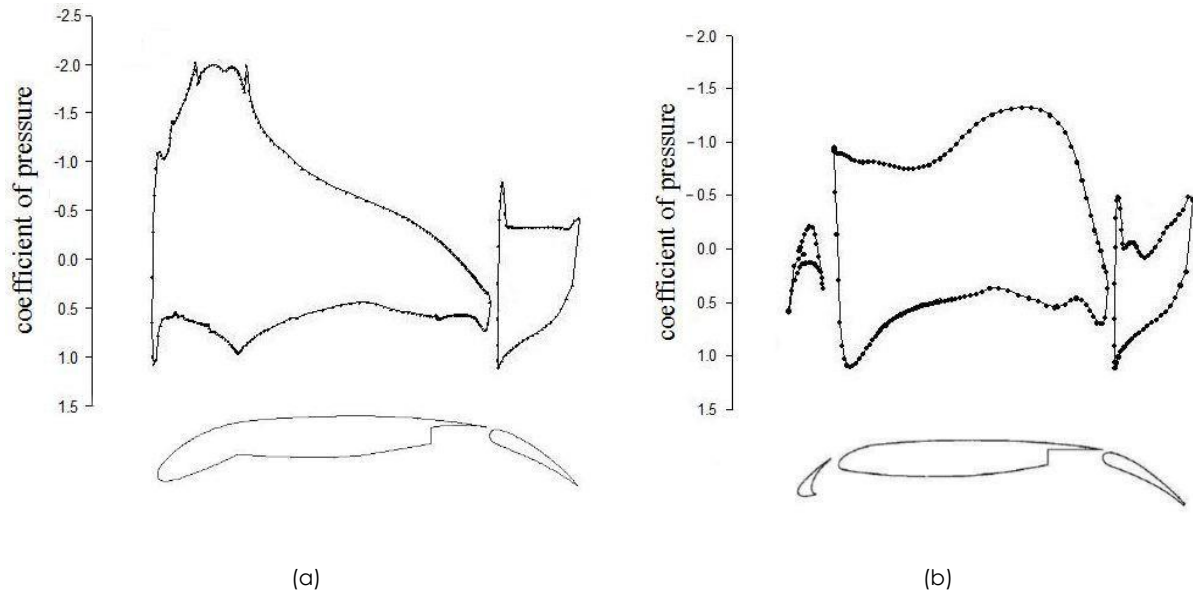
Figure 7 (a) Graph of coefficient of pressure, along the body of shape-changing airfoil (b) Graph of coefficient of pressure along the body of conventional airfoil

(a)   (b)
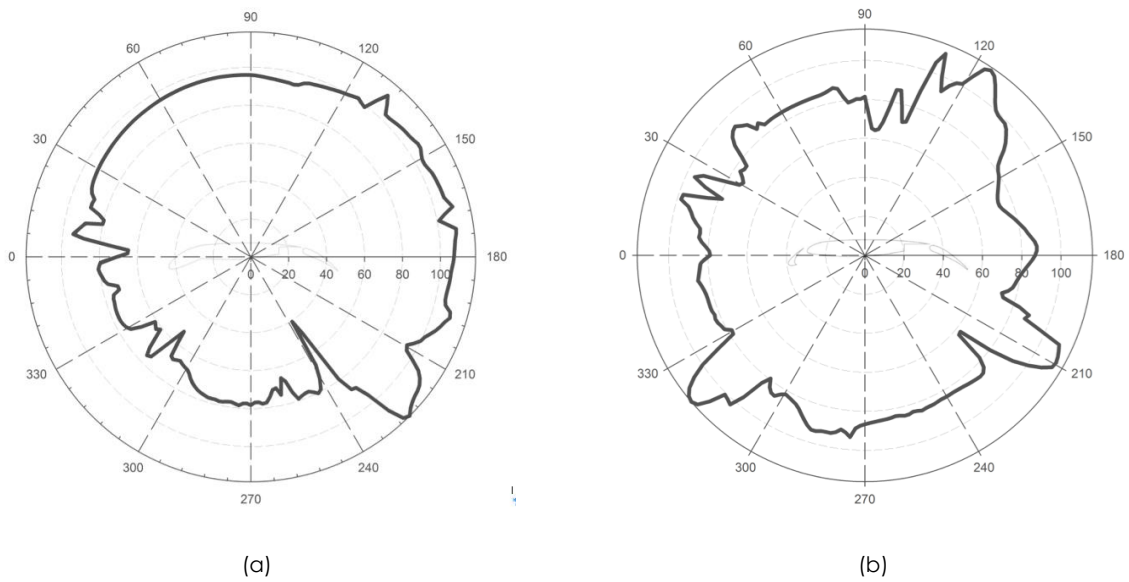
Figure 8 (a) Value of Sound Pressure Level, SPL (dB) over the shape-changing airfoil (b) Value of Sound Pressure Level, SPL (dB) over the conventional airfoil

5.0 CONCLUSION

In this paper, the new shape-change slat mechanism is proposed. In developing this mechanism, this work covers the following process:

a) The preliminary process to synthesize the shape-change slat mechanism where ShapeChanger is used to synthesize the segmentation process. CATIA software is applied along with GCP technique to design the slat profiles into solid model mechanism.

b) The 2D computational analysis is carried out for both conventional and shape-changing 30P30N airfoils to study the aerodynamic performance. The gap between the slat and main body not only affects the region close to the main body but also the stretches further toward the rear flap undergo other effects. The shape-changing airfoil covering the gap between the slat and main body possesses many benefits including lowering static pressure that can affect noise generation. As the air flew through the slat to main body, the values of static pressure and velocity are constant and controllable at the specified value. The values of SPL at the area of slat for both airfoils show the shape-changing airfoil has constant high and low SPL value at upper surface and lower surface while the conventional airfoil has inconsistent SPL value at both surfaces.

Acknowledgement

References

[1] Hayes, J. A., W. C., 1997, Soderman. P. T., and Bent, P.H., Airframe Noise Characteristics of a 4.7% Scale DC-10 Mode. *AIAA Paper*. 97-1594.

[2] Konig, D., Koh, S. R., Schroder, W., and Meinke, M., 2009, Slat Noise Identification. AIAA Paper. 2009-3100.

[3] Khorrami, M.R. 2003, Understanding Slat Noise Sources, Colloquium EUROMECH 449, Chamonix, France.

[4] Gaunaa, 2010, Unsteady Two-Dimensional Potential-Flow Model for Thin Variable Geometry Airfoils. *Wind Energy*. 12: 167-192.

[5] Morrison, J.H., 1998. Numerical Study of Turbulent Model Predictions for the MD 30P/30N and the NHLP-2D Three-Element Highlift Configurations, NASA CR-1998-208967.

[6] Weisshar, T.A. 2006. Morphing Aircraft Technology - New Shapes for Aircraft Design, *In Proceedings of the Multifunctional Structures Integration of Sensors and Antennas Meeting*. 1.

[7] Abdulrahim, M., Garcia, H., and Lind, R. 2005. Flight Characteristics of Shaping the Membrane Wing of a Micro Air Vehicle. *Journal of Aircraft*. 42: 131-137.

[8] Kota, S. and Hetrick, J. A. 2008, Adaptive Compliant Wing and Rotor System, U.S. Patent US7. 384, 016B2.

[9] Shamsudin, S. A. 2013. *Kinematic Synthesis Of Planar, Shape-Changing Rigid Body Mechanisms for Design Profiles with Significant Differences in Arc Length*. University of Dayton, Ohio, United States.

[10] Rumsey, C. L., and Ying, S. X., 2002. Prediction of High Lift: Review of Present CFD Capability. *Progress in Aerospace Sciences*. 38: 145-180.

[11] Fang, L., 2011. *Suppression Of Stall On High-Chamber Flap Using Upper-Surface Flow*. Cranfield University, Bedfordshire, United Kingdom, January.

[12] Zhao, K., Schmiedeler, J. P., and Murray, A. P., 2012. Design of Planar, Shape-Changing Rigid-Body Mechanisms for Morphing Aircraft Wings. *ASME Journal of Mechanisms and Robotics*. 4(4): 041007.

[13] Kinzel, G. L., and Chang, C., 1984. The Analysis of Planar Linkages Using a Modular Approach, Mech. Mach. *Theory*. 19(1):165–172.

[14] Myszka, D. H., Murray, A. P., and Schmiedeler, J. P., 2009. Singularity Analysis of an Extensible Kinematic Architecture: Assur Class N, Order N-1. *ASME J. Mech. Rob*. 1(1): 011009.

[15] Neville, A. B., and Sanderson, A. C., 1996. Tetrobot family tree: modular synthesis of kinematic structures for parallel robotics, *In Proc. IEEE/RSJ IROS*. Osaka, Japan.

[16] Krishnan, G., Kim, C., and Kota, S., 2011. An Intrinsic Geometric Framework for the Building Block Synthesis of Single Point Compliant Mechanisms. *ASME J. Mech. Rob*. 3(1): 011001.

[17] Kinzel, E. C., Schmiedeler, J. P., and Pennock, G. R., 2006. Kinematic Synthesis for Finitely Separated Positions Using Geometric Constraint Programming. *ASME J. Mech. Des*. 128(5): 1070–1079.

[18] Kintscher, M., Wiedemann, M., Monner, H. P., Heintze, O., and Kuhn, T., 2011. Design of a smart leading edge device for low speed wind tunnel tests in the European project SADE. *International Journal of Structural*. 4(4): 383-405.

[19] Pott-Pollenske, M., Wild, J., Herr, M., Delfs, J., 2014. Slat Noise Reduction by Means of Adaptive Leading Edge Devices, Aircraft Noise Reduction by Flow Control and Active/Adaptive Techniques, Vilnius, Lithuania, Sept. 25-26.